Eur. Phys. J. B **26**, 101–114 (2002)
DOI: 10.1140/epjb/e20020071

THE EUROPEAN PHYSICAL JOURNAL B
EDP Sciences

Transport theory of multiterminal hybrid structures

R. Mélin[1,a] and D. Feinberg[2]

[1] Centre de Recherches sur les Très Basses Températures (CRTBT)[b], CNRS BP 166X, 38042 Grenoble Cedex, France
[2] Laboratoire d'Études des Propriétés Électroniques des Solides, CNRS BP 166X, 38042 Grenoble Cedex, France

Received 18 June 2001 and Received in final form 17 January 2002

Abstract. We derive a microscopic transport theory of multiterminal hybrid structures in which a superconductor is connected to several spin-polarized electrodes. We discuss the non-perturbative physics of extended contacts, and show that such contacts can be well represented by averaging out the phase of the electronic wave function. The intercontact Andreev reflection and elastic cotunneling conductances are identical if the phase can be averaged out, namely in the presence of at least one extended contact. The maximal conductance of a two-channel contact is proportional to $(e^2/h)(a_0/D)^2 \exp[-D/\xi(\omega^*)]$, where D is the distance between the contacts, a_0 the lattice spacing, $\xi(\omega)$ is the superconducting coherence length, and ω^* is the cross-over frequency between a perturbative regime ($\omega < \omega^*$) and a non perturbative regime ($\omega^* < \omega < \Delta$).

PACS. 74.80.Fp Point contacts; SN and SNS junctions – 72.10.Bg General formulation of transport theory

1 Introduction

Transport of correlated pairs of electrons in multiterminal configurations has recently focused an important interest. One possible line of research is motivated by the possibility of creating entangled pairs of electrons from a superconductor [1–5]. This may lead to fundamental tests of quantum mechanics in solid state, or to new ways of manipulating quantum information. In a different context, the interplay between superconductivity and magnetism offers novel functionalities in multiterminal devices: the various transport channels occurring at several neighboring superconducting-ferromagnet interfaces depend in a subtle way on spin polarizations and geometry [6–10]. At the theoretical level, there is a need for a transport theory in multiterminal hybrid structures involving superconducting and spin-polarized elements. Several experiments have already been performed in multiterminal hybrid structures [11,12] but the specific structures that we consider in our article have not been yet the subject of experiments. As a consequence, one of the objective of the present time models is to predict what should be measured in future experiments.

In ferromagnet – superconductor junctions, it is well established that Andreev reflection is suppressed by an increase of spin polarization [6]. This is because Andreev reflection can take place only in the channels having both a spin-up and a spin-down Fermi point. This theoretical prediction has been probed experimentally by two independent groups [7,8]. Spin polarized Andreev reflection [7] and related effects [13] can even be used to measure the Fermi surface spin polarization.

We are concerned here with more sophisticated systems in which a superconductor is connected to several electrodes, which can be ferromagnetic or normal metals. In the case of ferromagnetic electrodes, it will be crucial to take into account the existence of a very small coherence length. We neglect any diffusive effect in spite of the fact that they lead to a rich physics [11,12,14,15]. As a consequence, our models should apply to point contacts having a dimension much smaller than the diffusive mean free path. The fabrication of such contacts in multiterminal configurations may seem difficult in view of the present day technology, and this is why there are no available experiments on these systems. However, there are interesting phenomena taking place in these multiterminal systems. For instance, Andreev reflection can become *non local*. Namely a spin-up electron from a given electrode A can be Andreev reflected as a hole in a *different* electrode B. This effect has been studied theoretically by Byers and Flatté in reference [16] for normal metals, and in reference [3] in the ferromagnetic case which contains the richest physics. It is in our opinion crucial to develop the most general theoretical description of this phenomenon. In this respect, two approaches have been developed recently. One is based on the analysis of the lowest order processes appearing in perturbation theory [4]. Another approach is non perturbative, but relies on effective Green's functions [5]. It is a very natural task to work out the microscopic theory of transport in ballistic multiterminal hybrid

[a] e-mail: melin@polycnrs-gre.fr
[b] U.P.R. 5001 du CNRS, Laboratoire conventionné avec l'Université Joseph Fourier

structures. Transport theory will be solved exactly by means of Green's function techniques [17]. We incorporate in our theoretical description the following features:

(i) *Multichannel effects* which are expected to play a central role in quantum point contacts involving ferromagnetic metals. The radius of the contact can be smaller or larger than the phase coherence length of the ferromagnetic metal.
(ii) *The strength of the tunnel amplitude* is small in low transparency contacts, and large in high transparency contacts. Our approach is non perturbative. Therefore, the tunnel matrix element can take arbitrary values. As a result, we can derive transport in the presence of arbitrary bias voltages.

An ingredient that is not incorporated at the present stage in the model is the reduction of the superconducting gap associated to the proximity effect.

It has been already established that the multiterminal hybrid system should be described by a *conductance matrix*. The matrix elements encode all information about the current flowing in a given electrode, in response to a voltage applied in another electrode. We determine the behavior of the crossed conductance when the voltages are close to the superconducting gap and determine the maximal value of the crossed conductance. The superconductor Green's functions contain not only an information about non local processes, but contain also an information about the phase of electron propagation. In extended contacts, there are many phases coming into account. We determine to what extend these phases can be considered as random quantities. There are two propagators associated to a superconductor: the ordinary and the anomalous propagators. One can easily realize that after phase averaging, the ordinary propagator is identical to the anomalous propagator (see Sect. 3.1.3). As a consequence, in the tunnel approach and for unpolarized contacts, the averaged Andreev reflection conductance is equal to the averaged elastic cotunneling conductance [4]. We show that this identity is still valid in the presence of large interface transparencies.

The article is organized as follows. Some preliminaries are given in Section 2. The form of the Green's functions is derived in Section 3. The solution of the model with two single-channel electrodes is presented in Section 4. The general solution with an arbitrary number of single-channel electrodes is presented in Section 5. As a particular example, we discuss in Section 6 the physics of a model with three single-channel electrodes. Multichannel electrodes are solved in Section 7.

2 Preliminaries

2.1 The Keldysh method

We will use Green's functions techniques to solve transport theory. There is an advanced ($\hat{G}^A$), retarded ($\hat{G}^R$) and Keldysh ($\hat{G}^{+,-}$) Green's functions [18,19]. Each of these Green's functions is a 2×2 matrix in Nambu representation. The Dyson equation for the advanced and retarded Green's functions takes the form

$$\hat{G}^{R,A} = \hat{g}^{R,A} + \hat{g}^{R,A} \otimes \hat{\Sigma} \otimes \hat{G}^{R,A}. \tag{1}$$

The Dyson equation for the Keldysh component is given by

$$\hat{G}^{+,-} = \left[\hat{I} + \hat{G}^R \otimes \hat{\Sigma}\right] \otimes \hat{g}^{+,-} \otimes \left[\hat{I} + \hat{\Sigma} \otimes \hat{G}^A\right] \cdot \tag{2}$$

Equations (1, 2) are written in a compact notation in which the convolution involves a summation over time variables and space labels. $\hat{\Sigma}$ is the self energy, which contains all couplings present in the tunnel Hamiltonian. The notation $\hat{g}$ is used for the Green's functions of the disconnected system (*i.e.* with $\hat{\Sigma}=0$) while $\hat{G}$ refers to the Green's functions of the connected system (*i.e.* with $\hat{\Sigma}\neq 0$). We will use the notation

$$\hat{g}^{A,R}(t,t') = \begin{pmatrix} g^{A,R}(t,t') & f^{A,R}(t,t') \\ f^{A,R}(t,t') & g^{A,R}(t,t') \end{pmatrix} \tag{3}$$

for the Nambu representation of the advanced and retarded Green's functions, with

$$g^A(t,t') = -\mathrm{i}\theta(t-t')\left\langle \left\{ c_{i,\uparrow}(t), c^+_{j,\uparrow}(t') \right\} \right\rangle \tag{4}$$

$$f^A(t,t') = -\mathrm{i}\theta(t-t')\langle\{c_{i,\uparrow}(t), c_{j,\downarrow}(t')\}\rangle\cdot \tag{5}$$

We will also denote by $\hat{\rho} = \frac{1}{\pi}\mathrm{Im}(\hat{g}^A)$ the Nambu representation of the density of states:

$$\hat{\rho} = \begin{pmatrix} \rho_g & \rho_f \\ \rho_f & \rho_g \end{pmatrix}, \tag{6}$$

with $\rho_g = \frac{1}{\pi}\mathrm{Im}(g^A)$ and $\rho_f = \frac{1}{\pi}\mathrm{Im}(f^A)$. The Nambu representation of a given tunnel matrix element connecting sites a and α is $t_{a,\alpha}\hat{\sigma}^z$, where $\hat{\sigma}^z$ is one of the Pauli matrices. We use a notation in which the "sites" of the superconductor are represented by the Greek symbols α, β , γ... The sites in the normal metal electrodes are represented by the Latin symbols a, b, c , ... The tunnel Hamiltonian takes the form

$$\hat{\mathcal{W}} = \sum_{k,\sigma} t_{a_k,\alpha_k}\left(c^+_{a_k,\sigma}c_{\alpha_k,\sigma} + c^+_{\alpha_k,\sigma}c_{a_k,\sigma}\right).$$

The explicit form of the Keldysh Green's function connecting the two sides of a given interface is, from (2)

$$\hat{G}^{+,-}_{\alpha_k,a_k} = \sum_{i,j}\left[\delta_{k,i}\hat{I} + \hat{G}^R_{\alpha_k,a_i}\hat{t}_{a_i,\alpha_i}\right]\hat{g}^{+,-}_{\alpha_i,\alpha_j}\hat{t}_{\alpha_j,a_j}\hat{G}^A_{a_j,a_k} + \sum_{i,j}\hat{G}^R_{\alpha_k,\alpha_i}\hat{t}_{\alpha_i,a_i}\hat{g}^{+,-}_{a_i,a_j}\left[\delta_{k,j}\hat{I} + \hat{t}_{a_j,\alpha_j}\hat{G}^A_{\alpha_j,a_k}\right]\cdot \tag{7}$$

The strategy is first to use (1) to calculate the advanced and retarded Green's functions and next use (2) to calculate the Keldysh Green's function. The current can be obtained easily from the Keldysh Green's function [19]:

$$I_{a_k,\alpha_k} = \frac{e}{h}\int \mathrm{d}\omega\left[\hat{t}_{a_k,\alpha_k}\hat{G}^{+,-}_{\alpha_k,a_k} - \hat{t}_{\alpha_k,a_k}\hat{G}^{+,-}_{a_k,\alpha_k}\right]\cdot \tag{8}$$

The spin-up (spin-down) current is given by the 11 (22) matrix element of the Nambu representation.

3 Form of the Green's functions

In this section, we present a derivation of the form of the Green's functions that will be used throughout the remainder of the article. This will give us the opportunity to discuss the relevant parameters of the model.

3.1 Green's functions in the superconductor

3.1.1 Effective Green's functions

In some cases, it will be useful to describe the superconducting and ferromagnetic reservoirs in terms of effective Green's functions. It was already shown by one of us in reference [5] that effective Green's functions can be used to construct a consistent non perturbative "toy model" version of transport theory. In this approach, the superconductor is viewed as zero dimensional: its dimensions are shorter than the coherence length. The superconducting effective Green's function takes the form [17]:

$$\hat{g}^{R,A}(\omega) = \frac{\pi\rho_N}{\sqrt{\Delta^2-(\omega-\mu_S)^2}} \times \begin{bmatrix} -(\omega-\mu_S)\pm \mathrm{i}\eta & \Delta \\ \Delta & -(\omega-\mu_S)\pm \mathrm{i}\eta \end{bmatrix}, \quad (9)$$

and we will consider in the following the limit $\eta \to 0$. The Keldysh component is given by $\hat{g}^{+,-}(\omega) = 2\mathrm{i}\pi n_F(\omega-\mu_S)\hat{\rho}(\omega)$, with $\hat{\rho}(\omega) = \frac{1}{\pi}\mathrm{Im}(\hat{g}^A)$ the density of states. The ferromagnetic electrodes are described in a similar way:

$$\hat{g}^{R,A} = \mp \mathrm{i}\pi \begin{bmatrix} \rho_{1,1} & 0 \\ 0 & \rho_{2,2} \end{bmatrix}, \quad (10)$$

where $\rho_{1,1}$ and $\rho_{2,2}$ are respectively the spin-up and spin-down densities of states.

3.1.2 Spectral representation

To address more realistic models, it is useful to restore the dependence of the Green's functions upon space coordinates. The Green's function are evaluated in terms of a spectral representation. Let us start with the pairing Hamiltonian

$$\mathcal{H} = \sum_{\boldsymbol{k},\sigma} \xi_k c^+_{\boldsymbol{k},\sigma} c_{\boldsymbol{k},\sigma} + \Delta^*_k c^+_{\boldsymbol{k},\downarrow} c^+_{\boldsymbol{k},\uparrow} + \Delta_k c_{\boldsymbol{k},\uparrow} c_{\boldsymbol{k},\downarrow}, \quad (11)$$

with $k = |\boldsymbol{k}|$. We use the notation $\xi_{\boldsymbol{k}} = \epsilon_{\boldsymbol{k}} - \mu$, with $\epsilon_{\boldsymbol{k}} = \hbar^2 k^2/(2m)$ for the kinetic energy.

3.1.3 Form of the Green's function

We now restrict our discussion to the case of a three dimensional superconductor. We first perform the angular integration and next use the residue theorem to make the radial integration in the spectral representation. Note that it is crucial to carry out first the angular integration. This ensures the existence of well defined convergence properties when we use the residue theorem to make the radial integration. The final result is

$$\hat{g}^{R,A}_{i,j}(\omega) = \frac{ma_0^3}{\hbar^2}\frac{1}{2\pi|\boldsymbol{x}_i-\boldsymbol{x}_j|}\exp\left(-\frac{|\boldsymbol{x}_i-\boldsymbol{x}_j|}{2\xi(\omega)}\right) \times \left\{ \frac{\sin\varphi}{\sqrt{\Delta^2-(\omega-\mu_S)^2}} \times \begin{bmatrix} -(\omega-\mu_S)\pm \mathrm{i}\eta & \Delta \\ \Delta & -(\omega-\mu_S)\pm \mathrm{i}\eta \end{bmatrix} - \cos\varphi \begin{bmatrix} 1 & 0 \\ 0 & 1 \end{bmatrix} \right\}, \quad (12)$$

with $\varphi = k_F|x_i - x_j|$ and a_0 is the length of the elementary cell. The coherence length appearing in (12) is

$$\xi(\omega) = \begin{cases} \xi(0)\frac{\Delta}{\sqrt{\Delta^2-\omega^2}} & \text{if } \omega < \Delta \\ +\infty & \text{if } \omega > \Delta. \end{cases} \quad (13)$$

We used the notation $\xi(0) = \frac{\epsilon_F}{k_F\Delta}$ for the zero-frequency coherence length, with ϵ_F the Fermi energy. In the case of two point contacts a and b treated explicitly in Section 4, the Green's function $g^{R,A}_{a,b}$ provides a coherent coupling between charge transport at the two contacts. We end-up this section with three remarks. First, we note that with $\cos\varphi = 0$ the Green's functions are identical to the effective Green's functions given in Section 3.1.1. Second, we recover the usual free-fermion Green's function in the limit $\omega \gg \Delta$:

$$g^R_{i,j}(\omega) = -\mathrm{i}\frac{ma_0^3}{\hbar^2}\frac{1}{2\pi|\boldsymbol{x}_i-\boldsymbol{x}_j|}\mathrm{e}^{\mathrm{i}k_F|\boldsymbol{x}_i-\boldsymbol{x}_j|}.$$

Finally, we will discuss in detail the role played by phase averaging. Using the notation $\langle\langle ...\rangle\rangle = \int \frac{\mathrm{d}\varphi}{2\pi}$, one can show that $\langle\langle (g_{i,j})^2\rangle\rangle = \langle\langle (f_{i,j})^2\rangle\rangle$. This identity implies that in the tunnel limit the average Andreev reflection conductance is equal to the average elastic cotunneling conductance.

3.2 Green's functions in the ferromagnetic electrodes

The Green's function in the ferromagnetic electrodes are diagonal in Nambu space. The form of the Green's function is taken as

$$g^R_{i,j,\sigma}(\omega) = -\mathrm{i}\frac{ma_0^3}{\hbar^2}\frac{1}{2\pi|\boldsymbol{x}_i-\boldsymbol{x}_j|}\exp\left(\mathrm{i}\varphi^{(\sigma)}\right) \times \exp\left(-\frac{|x_i-x_j|}{2l_\phi^{(\sigma)}}\right), \quad (14)$$

where the phase is given by $\varphi^{(\sigma)} = k_F^{(\sigma)}|x_i - x_j|$ and $l_\phi^{(\sigma)}$ is the phase coherence length. There is a mismatch between the spin-up and spin-down Fermi wave vectors:

$$k_F^{(\sigma)} = \frac{\sqrt{2m}}{\hbar}\sqrt{\epsilon_F + \sigma h_{\mathrm{ex}} + \omega},$$

where $h_{\rm ex}$ is the exchange field. At some point, it will be convenient to assume that the phase takes the particular value $\varphi^{(\sigma)} = 0$. With this special value of the phase, the form of the 3D Green's function (14) is identical to the effective Green's function (10). The coherence length in ferromagnetic metals is much shorter than in usual metals so that ferromagnetism is often treated in a semi-classical description (see [20–22]). For instance, the absence of Aharonov-Bohm oscillations reported in reference [11] shows that the coherence length in Co is smaller than 0.3 μm. This can be incorporated in our model by considering that the "dissipation" η is not a small parameter. This results in a finite coherence length, which is spin-dependent, and inverse proportional to the strength of dissipation:

$$l_\phi^{(\sigma)} = \frac{1}{\eta}\frac{\hbar}{\sqrt{2m}}\sqrt{\epsilon_F + \sigma h_{\rm ex} + \omega}.$$

This simple phenomenological model contains the relevant physics associated to ferromagnetic metals. For instance, the phase coherence length of spin-up electrons is larger than the spin-down coherence length. The Green's function (14) is infinite when $\boldsymbol{x}_i = \boldsymbol{x}_j$, which is also the case for the superconductor Green's function (12). Local quantities can be obtained by using $|\boldsymbol{x}_i - \boldsymbol{x}_j| = a_0$ instead of $\boldsymbol{x}_i = \boldsymbol{x}_j$. With this condition, the local density of states of the ferromagnet is given by

$$\rho^{(\sigma)} = \frac{1}{2\pi^2}\frac{ma_0^2}{\hbar^2}\exp\left(-\frac{a_0}{2l_\phi^{(\sigma)}}\right).$$

Spin-up electrons have thus a larger density of states than spin-down electrons.

4 Single channel electrodes: (I) two electrodes with 100% spin polarization

In this section, we consider a model in which a single channel spin-up electrode a and a single channel spin-down electrode b are in contact with a superconductor. We assume in Sections 4.1 and 4.2 that a is a spin-up channel and b is a spin-down channel. The result for parallel spin orientations is given in Section 4.3.

4.1 Derivation of the transport formula

4.1.1 Solution of the Dyson equation

Let us first calculate the Nambu representation of the propagators. The starting point is the chain of Dyson equations given by (1):

$$\begin{bmatrix}\hat{G}^{a,a}\\ \hat{G}^{b,a}\end{bmatrix} = \begin{bmatrix}g^{a,a}\\ 0\end{bmatrix} + \begin{bmatrix}\hat{K}^{a,a} & \hat{K}^{a,b}\\ \hat{K}^{b,a} & \hat{K}^{b,b}\end{bmatrix}\begin{bmatrix}\hat{G}^{a,a}\\ \hat{G}^{b,a}\end{bmatrix}, \tag{15}$$

where we used the notation $\hat{K}^{a_i,a_j} = \hat{g}^{a_i,a_i}\ \hat{t}^{a_i,\alpha_i}\ \hat{g}^{\alpha_i,\alpha_i'}\ \hat{t}^{\alpha_i',a_i'}$. The solution of equation (15) is

$$\begin{bmatrix}G_{1,1}^{a,a} & G_{1,2}^{a,b}\\ G_{2,1}^{b,a} & G_{2,2}^{b,b}\end{bmatrix} = \frac{1}{\mathcal{D}_{\rm AF}} \times \begin{bmatrix} g_{1,1}^{a,a}\left[1-|t^{b,\beta}|^2 g_{2,2}^{b,b} g^{\beta,\beta}\right] & -g_{2,2}^{b,b} t^{a,\alpha} t^{b,\beta} g_{1,1}^{a,a} f^{\alpha,\beta}\\ -g_{a,a}^{1,1} t^{a,\alpha} t^{b,\beta} g_{2,2}^{b,b} f^{\beta,\alpha} & g_{2,2}^{b,b}\left[1-|t^{a,\alpha}|^2 g_{1,1}^{a,a} g^{\alpha,\alpha}\right]\end{bmatrix}, \tag{16}$$

where the determinant $\mathcal{D}_{\rm AF}$ is given by

$$\mathcal{D}_{\rm AF} = \left[1-|t^{a,\alpha}|^2 g_{1,1}^{a,a} g^{\alpha,\alpha}\right]\left[1-|t^{b,\beta}|^2 g_{2,2}^{b,b} g^{\beta,\beta}\right] - |t^{a,\alpha}|^2 |t^{b,\beta}|^2 g_{1,1}^{a,a} g_{2,2}^{b,b} f^{\alpha,\beta} f^{\beta,\alpha}, \tag{17}$$

and g and f have been defined as the components of the Nambu matrix in (3) and (12). If not specified, all Green's functions in a given formula stand as well for advanced and retarded functions, and similarly for the determinant $\mathcal{D}_{\rm AF}$ given by equation (17) and the determinant $\mathcal{D}_{\rm F}$ that will be introduced latter. The matrix in equation (16) contains the non vanishing Nambu components of the renormalized propagator. Because we assume a complete spin polarization, the other Nambu components are vanishing. For instance $G_{1,2}^{a,a} = G_{2,1}^{a,a} = G_{2,2}^{a,a} = 0$.

4.2 Exact expression of the current

Using the expression of the Keldysh propagator (see Appendix A), we deduce the final expression of the spin-up current in electrode a:

$$I_{1,1}^{a,\alpha} = -4\pi^2|t_{a,\alpha}|^2 \int {\rm d}\omega\,[n_F(\omega-\mu_a) - n_F(\omega-\mu_S)]\,\rho_{1,1}^{a,a}\rho_g^{\alpha,\alpha} \tag{18}$$

$$\times \frac{1}{\mathcal{D}^A\mathcal{D}^R}\left[1-|t_{b,\beta}|^2 g_{2,2}^{b,b,A} g^{\beta,\beta,A}\right]\left[1-|t_{b,\beta}|^2 g_{2,2}^{b,b,R} g^{\beta,\beta,R}\right]$$

$$+ 2{\rm i}\pi|t_{a,\alpha}|^2|t_{b,\beta}|^2 \times \int {\rm d}\omega\,[n_F(\omega-\mu_a) - n_F(\omega-\mu_S)]\,\rho_{1,1}^{a,a} g_{2,2}^{b,b,A} \tag{19}$$

$$\times \frac{1}{\mathcal{D}^A\mathcal{D}^R} f^{\alpha,\beta,A} f^{\beta,\alpha,A}\left[1-|t_{b,\beta}|^2 g_{2,2}^{b,b,R} g^{\beta,\beta,R}\right]$$

$$- 2{\rm i}\pi|t_{a,\alpha}|^2|t_{b,\beta}|^2 \times \int {\rm d}\omega\,[n_F(\omega-\mu_a) - n_F(\omega-\mu_S)]\,\rho_{1,1}^{a,a} g_{2,2}^{b,b,R} \tag{20}$$

$$\times \frac{1}{\mathcal{D}^A\mathcal{D}^R} f^{\alpha,\beta,R} f^{\beta,\alpha,R}\left[1-|t_{b,\beta}|^2 g_{2,2}^{b,b,A} g^{\beta,\beta,A}\right]$$

$$- 4\pi^2|t_{a,\alpha}|^2|t_{b,\beta}|^2 \int {\rm d}\omega\,[n_F(\omega-\mu_b) - n_F(\omega-\mu_S)] \times \frac{1}{\mathcal{D}^A\mathcal{D}^R}\rho_{1,1}^{a,a}\rho_{2,2}^{b,b} f^{\alpha,\beta,R} f^{\beta,\alpha,A}, \tag{21}$$

which generalizes the result obtained by Cuevas *et al.* in reference [17] in the case of a single conduction channel. From the density of state prefactors, we see that there are

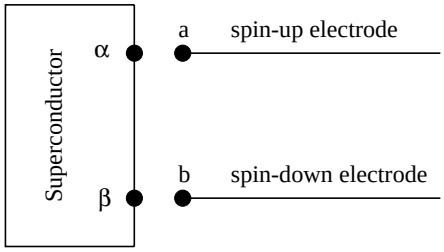

Fig. 1. Schematic representation of the model considered in Section 4. Two ferromagnetic electrodes are in contact with a superconductor. A voltage V_S is applied on the superconductor while the voltages V_a and V_b are applied on the ferromagnetic electrodes.

two type of contributions to the current: (i) *The quasiparticle current*, which is proportional to the product of the density of state in the superconductor (ρ_g) and one of the ferromagnetic electrodes (for instance ρ_a); (ii) *The crossed Andreev current* which is proportional to the product $\rho_a\rho_b$ of the density of state in the two ferromagnetic electrodes. The term (18) contributes only to quasiparticle current. The term (21) contributes only to Andreev reflection. The mixed terms (19–20) contribute both to the quasiparticle and Andreev current.

4.3 Two-terminal conductance matrix

To understand the meaning of the transport formula (18), it is useful to describe transport across the multiterminal structure in terms of a differential conductance matrix:

$$\hat{\mathcal{G}} = \begin{bmatrix} \mathcal{G}_{a,a} & \mathcal{G}_{a,b} \\ \mathcal{G}_{b,a} & \mathcal{G}_{b,b} \end{bmatrix}, \tag{22}$$

where the matrix elements are given by

$$\mathcal{G}_{a_i,a_j}(V_a,V_b) = \frac{\partial I_{a_i}}{\partial V_{a_j}}(V_a,V_b). \tag{23}$$

The conductance matrix (22) encodes all information about transport in the two-terminal structure. The off-diagonal matrix elements should satisfy a symmetry relation: $\mathcal{G}_{a,b}(V_a,V_b) = \mathcal{G}_{b,a}(V_b,V_a)$. If the electrodes have an antiparallel spin orientation, subgap current is transported by Cooper pairs if $\omega < \Delta$, in which case we have $I_a = I_b$. This implies an additional symmetry relation: $\mathcal{G}_{a,a}(V_a,V_b) = \mathcal{G}_{b,a}(V_a,V_b)$, and $\mathcal{G}_{b,b}(V_a,V_b) = \mathcal{G}_{a,b}(V_a,V_b)$. If the electrodes have a parallel spin orientation, subgap current is due to elastic cotunneling, in which case $I_a = -I_b$. The additional symmetry relation reads $\mathcal{G}_{a,a}(V_a,V_b) = -\mathcal{G}_{b,a}(V_a,V_b)$, and $\mathcal{G}_{b,b}(V_a,V_b) = -\mathcal{G}_{a,b}(V_a,V_b)$.

4.3.1 Sub-gap conductance matrix: effective Green's functions

In this section as well as in Section 4.3.2, we assume that $\cos\varphi = 0$ so that we can use effective Green's functions to evaluate the transport formula and work out the basic physics on simple grounds. The validity of this assumption will be discussed in Section 4.4.

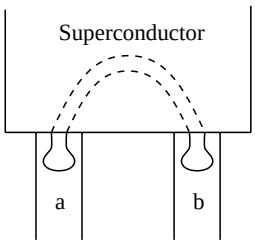

Fig. 2. The diagram associated to Andreev reflection in the two-channel model.

Antiparallel magnetizations:

The sub-gap current of the two-channel model with antiparallel magnetizations originates from the non local Andreev reflections which are shown schematically in Figure 2. This can be seen by inserting the effective Green's functions into the transport formula:

$$\mathcal{G}_{a,a} = \mathcal{G}_{b,a} = -\frac{4\Gamma_a\Gamma_b}{|\mathcal{D}_{\rm AF}(\omega=V_a)|^2}\left[f^{\alpha,\beta}(\omega=V_a)\right]^2 \tag{24}$$

$$\mathcal{G}_{a,b} = \mathcal{G}_{b,b} = -\frac{4\Gamma_a\Gamma_b}{|\mathcal{D}_{\rm AF}(\omega=V_b)|^2}\left[f^{\alpha,\beta}(\omega=V_b)\right]^2, \tag{25}$$

where $\Gamma_a = \pi|t_{a,\alpha}|^2\rho_a$ is the spectral line-width associated to electrode a, and a similar expression holds for Γ_b. We used the fact that $g^{\alpha,\beta}$ and $f^{\alpha,\beta}$ are real numbers below the superconducting gap. The expression of $\mathcal{D}_{\rm AF}$ is the following:

$$|\mathcal{D}_{\rm AF}(\omega)|^2 = \left\{1 - \Gamma^a\Gamma^b\left[g^{\alpha,\alpha}g^{\beta,\beta} - \left(f^{\alpha,\beta}\right)^2\right]\right\}^2 + \left(\Gamma^a g^{\alpha,\alpha} + \Gamma^b g^{\beta,\beta}\right)^2. \tag{26}$$

Parallel magnetizations:

The same calculation can be done if the electrodes have a parallel spin orientation. We find

$$\mathcal{G}_{a,a} = -\mathcal{G}_{b,a} = -\frac{4\Gamma_a\Gamma_b}{|\mathcal{D}_{\rm F}(\omega=V_a)|^2}\left[g^{\alpha,\beta}(\omega=V_a)\right]^2 \tag{27}$$

$$-\mathcal{G}_{a,b} = \mathcal{G}_{b,b} = -\frac{4\Gamma_a\Gamma_b}{|\mathcal{D}_{\rm F}(\omega=V_b)|^2}\left[g^{\alpha,\beta}(\omega=V_b)\right]^2, \tag{28}$$

with

$$|\mathcal{D}_{\rm F}(\omega)|^2 = \left\{1 - \Gamma^a\Gamma^b\left[g^{\alpha,\alpha}g^{\beta,\beta} - (g^{\alpha,\beta})^2\right]\right\}^2 + \left(\Gamma^a g^{\alpha,\alpha} + \Gamma^b g^{\beta,\beta}\right)^2. \tag{29}$$

There are two differences between the situations with antiparallel and parallel spin orientations. First, the Andreev reflection transport with antiparallel spin orientations is controlled by the anomalous propagator $f^{\alpha,\beta}$ while the elastic cotunneling transport with parallel spin orientations is controlled by the ordinary propagator $g^{\alpha,\beta}$. The

second difference is in the sign of the off-diagonal conductance matrix elements. The four matrix elements have the same sign in the case of Andreev reflection because transport is mediated by Cooper pairs. The off-diagonal matrix elements have a sign opposite to the diagonal matrix elements in the case of elastic cotunneling because transport is due to single electron tunneling between the two electrodes.

4.3.2 Conductance matrix above the superconducting gap: effective Green's functions

Let us now assume that the voltage V_a is above the superconducting gap and that the electrodes have an antiparallel spin orientation. With the notation $g^{\alpha,\beta,A,R} = \pm \mathrm{i}|g^{\alpha,\beta}|$, and $f^{\alpha,\beta,A,R} = \pm \mathrm{i}|f^{\alpha,\beta}|$, the extra diagonal terms of the conductance matrix take the form

$$\mathcal{G}_{b,a} = -\frac{4\Gamma_a\Gamma_b}{\mathcal{D}_{\rm AF}^2}|f^{\alpha,\beta}|^2,$$

which should be evaluated at the energy $\omega = V_a$. The diagonal conductance matrix element is the sum of a crossed contribution and a quasiparticle contribution: $\mathcal{G}_{a,a} = -\mathcal{G}_{b,a} - \mathcal{G}^{qp}_{a,a}$. The quasiparticle contribution is the sum of a direct and a crossed term:

$$\mathcal{G}^{qp}_{a,a} = \frac{4\pi\Gamma_a\rho_g}{\mathcal{D}_{\rm AF}^2}\left[\left(1+\Gamma_b|g^{\beta,\beta}|\right)^2 - \Gamma_b^2|f^{\alpha,\beta}|^2\right], \qquad (30)$$

where the denominator $\mathcal{D}_{\rm AF}$ is a real number:

$$\mathcal{D}_{\rm AF} = \mathcal{D}^A_{\rm AF} = \mathcal{D}^R_{\rm AF} = 1 + \Gamma^a\Gamma^b\left[|g^{\alpha,\alpha}g^{\beta,\beta}| - |f^{\alpha,\beta}|^2\right] + \Gamma^a|g^{\alpha,\alpha}| + \Gamma^b|g^{\beta,\beta}|.$$

In the limit $|\boldsymbol{x}_a - \boldsymbol{x}_b| \to +\infty$ in which the separation between the contacts becomes very large, the extra diagonal conductance matrix elements are vanishingly small. The quasiparticle term reduces to the conductance of a single channel metal – metal contact:

$$\mathcal{G}^{qp}_{a,a} = \frac{4\pi\Gamma_a\rho_g}{\left(1+\Gamma_a|g^{\alpha,\alpha}|\right)^2}.$$

4.4 Phase resolved versus averaged conductance

Given the form (12) of the superconductor Green's function, we see that the conductance depends explicitly on the electronic phase difference $\varphi = k_F|\boldsymbol{x}_a - \boldsymbol{x}_b|$. This leads us to calculate the conductance in two different ways:

(i) The phase-resolved conductance $\mathcal{G}(\varphi)$. We will focus more especially on the case $\varphi = \pi/2$. For this special value of the phase difference, the Green's function of the superconductor coincides with the effective Green's function in the limit $|\boldsymbol{x}_a - \boldsymbol{x}_b| \to a_0$.

(ii) The averaged conductance

$$\langle\langle\mathcal{G}(\varphi)\rangle\rangle = \frac{1}{2\pi}\int_0^{2\pi}\mathcal{G}(\varphi)\mathrm{d}\varphi. \qquad (31)$$

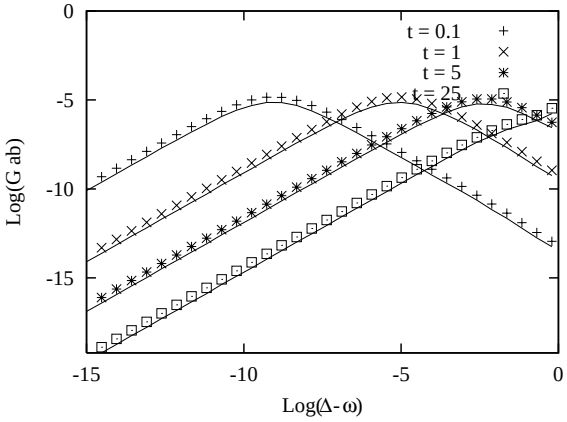

Fig. 3. Variation of the logarithm of the crossed conductance $\log\mathcal{G}_{a,b}$ *versus* $\log(\Delta-\omega)$ ($\omega < \Delta$). $\mathcal{G}_{a,b}$ is in units of e^2/h. The points correspond to the phase-resolved conductance with $\varphi = \pi/2$, namely, to the generalized effective Green's functions. The solid lines correspond to the average conductance (31). We used the parameters $m = 0.01$, $k_F = 1$, $\epsilon_F = 50$, $a_0 = 1$, $\Delta = 1$. The distance between the contacts is $D = 100$ and the superconductor coherence length is $\xi_0 = \epsilon_F/(k_F\Delta) = 50$.

This phase averaging is used to mimic the physics of extended contacts that will be considered later in Section 7.

To determine the role played by phase averaging, we compare the phase-dependent and average conductances (see the end of Sect. 3). It is visible in Figure 3 that the effective Green's function conductance (*i.e.* with $\varphi = \pi/2$) follows closely the average conductance. This shows that the effective Green's function conductance contains already the relevant physics, as far as the two-channel problem is concerned.

It is also visible in Figure 3 that there is a cross-over energy ω^* (thus a cross-over voltage $V^* = \omega^*/e$) at which the crossed conductance reaches a maximum. If $\omega < \omega^*$ the crossed conductance behaves like $\mathcal{G}_{a,b} \sim 1/(\Delta-\omega)$. If $\omega^* < \omega < \Delta$, the crossed conductance behaves like $\mathcal{G}_{a,b} \sim \Delta - \omega$. Only when $\omega < \omega^*$ does our approach coincide with the lowest order tunnel perturbation theory. The analysis based on generalized effective Green's functions is simplified if one assumes that $D \gg a_0$, but D can be small or large compared to the superconducting coherence length $\xi(\omega)$ (see Eq. (13)). The behavior in the energy range $\omega^* < \omega < \Delta$ is non perturbative, and can be understood by retaining in $\mathcal{D}_{\rm AF}$ only the leading divergence, which is generated by the quartic terms (see Eq. (26)):

$$|\mathcal{D}_{\rm AF}|^2 \simeq \Gamma^4\left[g^{\alpha,\alpha}g^{\beta,\beta} - \left(f^{\alpha,\beta}\right)^2\right]^2,$$

from what we deduce the expression of the crossed conductance

$$\mathcal{G}_{a,b} \simeq \frac{4}{\Gamma^2}\left(\frac{a_0}{D}\right)^2\left(\frac{2\pi\hbar^2}{ma_0^2}\right)^2\left(\frac{\Delta^2-\omega^2}{\Delta^2}\right)\exp\left(-\frac{D}{\xi(\omega)}\right), \qquad (32)$$

valid in the energy range $\omega > \omega^*$. The expression of the cross-over energy ω^* is obtained by equating the quadratic

$$I^{\alpha_1,a_1} = -4\pi^2|t^{a_1,\alpha_1}|^2\int \mathrm{d}\omega\,[n_F(\omega-\mu_{a_1})-n_F(\omega-\mu_S)]\,\rho^{\alpha_1,\alpha_1}\rho_g^{\alpha_1,\alpha_1}\frac{1}{\mathcal{D}^A\mathcal{D}^R}\tilde{\mathcal{M}}^A_{a_1,a_1}\tilde{\mathcal{M}}^R_{a_1,a_1} \tag{38}$$

$$-2\mathrm{i}\pi\sum_{k=2}^{N}(-)^{k+1}t^{a_1,\alpha_1}t^{a_k,\alpha_k}\int \mathrm{d}\omega\,[n_F(\omega-\mu_{a_1})-n_F(\omega-\mu_S)] \tag{39}$$

$$\times\frac{1}{\mathcal{D}^A\mathcal{D}^R}\left(g^{\alpha_1,\alpha_k,R}\tilde{\mathcal{M}}^R_{a_1,a_k}\tilde{\mathcal{M}}^A_{a_1,a_1}-g^{\alpha_1,\alpha_k,A}\tilde{\mathcal{M}}^A_{a_1,a_k}\tilde{\mathcal{M}}^R_{a_1,a_1}\right)$$

$$-2\mathrm{i}\pi\sum_{k=2}^{N}(-)^{k+N}t^{a_1,\alpha_1}t^{b_k,\beta_k}\int_{\mu_{a_1}}^{\mu_\alpha}\mathrm{d}\omega\,[n_F(\omega-\mu_{a_1})-n_F(\omega-\mu_S)] \tag{40}$$

$$\times\frac{1}{\mathcal{D}^A\mathcal{D}^R}\left(f^{\alpha_1,\beta_k,R}\tilde{\mathcal{M}}^R_{a_1,b_k}\tilde{\mathcal{M}}^A_{a_1,a_1}-f^{\alpha_1,\beta_k,A}\tilde{\mathcal{M}}^A_{a_1,b_k}\tilde{\mathcal{M}}^R_{a_1,a_1}\right)$$

$$+4\pi^2\sum_{k=2}^{N}|t^{a_1,\alpha_1}|^2|t^{a_k,\alpha_k}|^2\int \mathrm{d}\omega\,[n_F(\omega-\mu_{a_k})-n_F(\omega-\mu_S)] \tag{41}$$

$$\times\rho_{1,1}^{a_1,a_1}\rho_{1,1}^{a_k,a_k}\tilde{g}^{\alpha_1,\alpha_k,R}\tilde{g}^{\alpha_k,\alpha_1,A}-4\pi^2\sum_{k=1}^{M}|t^{a_1,\alpha_1}|^2|t^{b_k,\beta_k}|^2\int \mathrm{d}\omega\,[n_F(\omega-\mu_{b_k})-n_F(\omega-\mu_S)] \tag{42}$$

$$\times\rho_{1,1}^{a_1,a_1}\rho_{2,2}^{b_k,b_k}\tilde{f}^{\alpha_1,\beta_k,R}\tilde{f}^{\beta_k,\alpha_1,A},$$

and quartic terms in $\mathcal{D}_{\mathrm{AF}}$. This leads to

$$\omega^* = \Delta\sqrt{1-\left(\Gamma\frac{ma_0^2}{2\pi\hbar^2}\right)^2}\,. \tag{33}$$

To obtain the conductance in the energy range $\omega<\omega^*$, we expand $\mathcal{D}_{\mathrm{AF}}$ up to order Γ^2:

$$|\mathcal{D}_{\mathrm{AF}}|^2 \simeq 1+2\Gamma^2\left(g^{\mathrm{loc}}\right)^2+2\Gamma^2\left(f^{\alpha,\beta}\right)^2,$$

where $g^{\mathrm{loc}}=g^{\alpha,\alpha}=g^{\beta,\beta}$ denotes the local propagator in the superconductor. One can show easily that $f^{\alpha,\beta}\ll g^{\mathrm{loc}}$ because $D\gg a_0$, from what we deduce

$$|\mathcal{D}_{\mathrm{AF}}|^2 \simeq 1+2\Gamma^2\left(\frac{ma_0^2}{2\pi\hbar^2}\right)^2\frac{\omega^2}{\Delta^2-\omega^2}\,. \tag{34}$$

$\mathcal{D}_{\mathrm{AF}}$ is close to unity only when $\omega<\omega_0$, with

$$\omega_0 = \frac{\Delta}{\sqrt{1+2\Gamma^2\left(\frac{ma_0^2}{2\pi\hbar^2}\right)^2}}\,. \tag{35}$$

Comparing (33) and (35), we see that ω^* is larger than ω_0 but ω_0 and ω^* have the same order of magnitude is Γ is small (which is the case in Fig. 3). We deduce that $\mathcal{D}_{\mathrm{AF}}=1$ in the relevant energy range $\omega<\omega_0<\omega^*$. From what we obtain the conductance in the energy range $\omega<\omega_0$:

$$\mathcal{G}_{a,b} = 4\Gamma^2\left(\frac{a_0}{D}\right)^2\left(\frac{ma_0^2}{2\pi\hbar^2}\right)^2\frac{\Delta^2}{\Delta^2-\omega^2}\exp\left(-\frac{D}{\xi(\omega)}\right), \tag{36}$$

identical to the one obtained in lowest order perturbation theory. Evaluating (32) and (36) at $\omega=\omega^*$ or $\omega=\omega_0$ leads to the maximal value of the conductance:

$$\mathcal{G}_{a,b}^{\max} \simeq \frac{e^2}{h}\left(\frac{a_0}{D}\right)^2\exp\left(-\frac{D}{\xi(\omega^*)}\right), \tag{37}$$

where the numerical prefactor of order unity cannot be obtained from this simple estimate.

It is well known from the BTK scattering approach [23] that the conductance of a normal metal – superconductor contact is equal to twice the quantum of conductance e^2/h per spin channel if $\omega=\Delta$, *regardless the value of the interface scattering*. The same behavior occurs in the Keldysh formalism treatment by Cuevas *et al.* [17]. This type of resonance can be properly described only with a non perturbative approach. Equation (37) constitutes a generalization of the BTK behavior to the case of spatially separated contacts having a phase difference $\varphi=\pi/2$. Given that the average and phase-resolved conductances follow closely each other (see Fig. 3), it is expected that (37) is also valid for the average conductance, but with an extra reduction factor.

5 Single channel electrodes: (II) general solution

Now we consider a model in which N spin-up electrodes and M spin-down electrodes are in contact with a superconductor (see Fig. 4). All the necessary details can be found in Appendix B. The final form of the current is

See equations (38–42) above

where we used the notation

$$\tilde{g}^{\alpha_i,\alpha_j} = \frac{\tilde{\mathcal{M}}_{a_j,a_i}}{t^{a_i,\alpha_i}t^{a_j,\alpha_j}g^{a_i,a_i}\mathcal{D}} \tag{43}$$

$$\tilde{f}^{\alpha_i,\beta_j} = \frac{\tilde{\mathcal{M}}_{b_j,a_i}}{t^{a_i,\alpha_i}t^{b_j,\beta_j}g^{a_i,a_i}\mathcal{D}} \tag{44}$$

for the renormalized propagators. There are three types of processes involved in the transport formula: (i) *The quasiparticle term* (38) which is proportional to $\rho^{\alpha_1,\alpha_1}\rho_g$;

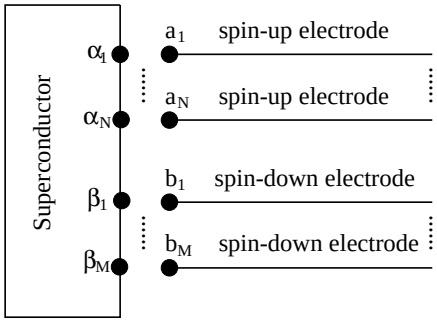

Fig. 4. Schematic representation of the model with N ferromagnetic spin-up electrodes and M ferromagnetic spin-down electrodes.

(ii) *The elastic cotunneling term* (41) in which spin-up electrons from electrode a_k are transfered into electrode 1. The elastic cotunneling terms are proportional to $\rho_{1,1}^{a_1,a_1}\rho_{1,1}^{a_k,a_k}$ (iii) *The Andreev reflection term* (42) which are proportional to $\rho_{1,1}^{a_1,a_1}\rho_{2,2}^{b_k,b_k}$. The mixed terms (39) and (40) contribute the three types of processes.

6 Single channel electrodes: (III) three electrodes with 100% spin polarization

Let us now consider a three-terminal problem. We consider that each of the three electrodes has 100% spin polarization (see Fig. 5). The aim is to have Andreev and cotunneling processes occurring in the same multiterminal device, which allows a direct comparison of these two basic processes. The transport formula can be deduced easily from the general solution obtained in Section 5.

6.1 Three-terminal conductance matrix

The three-terminal conductance matrix generalizing (22) takes the form

$$\hat{\mathcal{G}} = \begin{bmatrix} \mathcal{G}_{a,a} & \mathcal{G}_{a,b} & \mathcal{G}_{a,c} \\ \mathcal{G}_{b,a} & \mathcal{G}_{b,b} & \mathcal{G}_{b,c} \\ \mathcal{G}_{c,a} & \mathcal{G}_{c,b} & \mathcal{G}_{c,c} \end{bmatrix} . \tag{45}$$

Let us assume that electrode a has a spin-up magnetization, and electrodes b and c have a spin-down magnetization (see Fig. 5). We use the same procedure as in Section 4.3.1 to obtain the conductance matrix elements. Namely, we assume that $\cos\varphi = 0$ and replace the Green's functions by effective Green's functions.

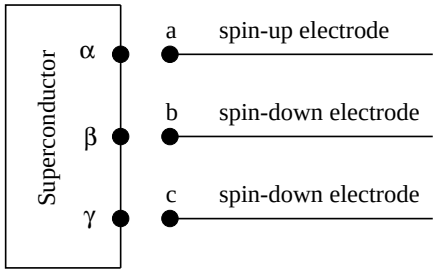

Fig. 5. Schematic representation of the three channel model considered in Section 6.

6.1.1 Conductance matrix below the superconducting gap: effective Green's functions

Let us first give the form of the off diagonal matrix elements:

$$\mathcal{G}_{a,b} = \mathcal{G}_{b,a} = -\frac{4\Gamma_a\Gamma_b}{\mathcal{D}^A\mathcal{D}^R} \times \left[\left(f^{\alpha,\beta}\right)^2 + \Gamma_c^2\left(f^{\alpha,\gamma}g^{\beta,\gamma} - f^{\alpha,\beta}g^{\gamma,\gamma}\right)^2\right] \tag{46}$$

$$\mathcal{G}_{a,c} = \mathcal{G}_{c,a} = -\frac{4\Gamma_a\Gamma_c}{\mathcal{D}^A\mathcal{D}^R} \times \left[\left(f^{\alpha,\gamma}\right)^2 + \Gamma_b^2\left(f^{\alpha,\beta}g^{\beta,\gamma} - f^{\alpha,\gamma}g^{\beta,\beta}\right)^2\right] \tag{47}$$

$$\mathcal{G}_{b,c} = \mathcal{G}_{c,b} = \frac{4\Gamma_b\Gamma_c}{\mathcal{D}^A\mathcal{D}^R} \times \left[\left(g^{\beta,\gamma}\right)^2 + \Gamma_a^2\left(f^{\alpha,\beta}f^{\alpha,\gamma} - g^{\alpha,\alpha}g^{\beta,\gamma}\right)^2\right] . \tag{48}$$

From the signs of these matrix elements, and from the type of propagator involved, we see that $\mathcal{G}_{a,b}$ and $\mathcal{G}_{a,c}$ correspond to Andreev reflection while $\mathcal{G}_{b,c}$ corresponds to elastic cotunneling.

6.1.2 Conductance matrix above the superconducting gap: effective Green's functions

Using the notation $f^{A,R} = \pm\mathrm{i}|f|$, and $g^{A,R} = \pm\mathrm{i}|g|$, we obtain the conductance matrix elements above the superconducting gap:

$$\mathcal{G}_{a,b} = \mathcal{G}_{b,a} = -\frac{4\Gamma_a\Gamma_b}{\mathcal{D}^A\mathcal{D}^R} \times \left[|f^{\alpha,\beta}| + \Gamma_c\left(|f^{\alpha,\beta}g^{\gamma,\gamma}| - |f^{\alpha,\gamma}g^{\beta,\gamma}|\right)\right]^2 \tag{49}$$

$$\mathcal{G}_{a,c} = \mathcal{G}_{c,a} = -\frac{4\Gamma_a\Gamma_c}{\mathcal{D}^A\mathcal{D}^R} \times \left[|f^{\alpha,\gamma}| + \Gamma_b\left(|f^{\alpha,\gamma}g^{\beta,\beta}| - |f^{\alpha,\beta}g^{\beta,\gamma}|\right)\right]^2 \tag{50}$$

$$\mathcal{G}_{b,c} = \mathcal{G}_{c,b} = -\frac{4\Gamma_b\Gamma_c}{\mathcal{D}^A\mathcal{D}^R} \times \left[|g^{\beta,\gamma}| + \Gamma_a\left(|g^{\beta,\gamma}g^{\alpha,\alpha}| - |f^{\alpha,\beta}f^{\alpha,\gamma}|\right)\right]^2 . \tag{51}$$

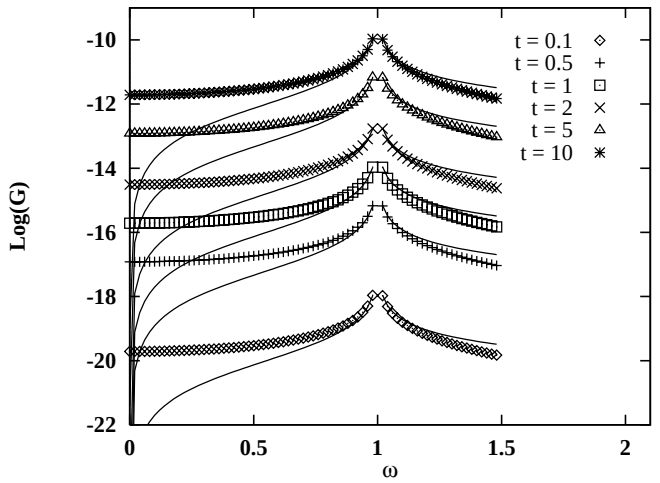

Fig. 6. Variation of the logarithm of the Andreev reflection conductance $\mathcal{G}_{a,c}$ and elastic cotunneling conductance $\mathcal{G}_{b,c}$ *versus* reduced energy ω/Δ. The points correspond to Andreev reflection and the solid lines correspond to elastic cotunneling. We have assumed that site α coincides with site β (see Fig. 5). We used effective Green's functions with $\varphi = \pi/2$. The distance between the contacts is $D = 100$. On purpose, we did not show the behavior for $\omega \simeq \Delta$ (see Fig. 7). The parameters are identical as in Figure 3.

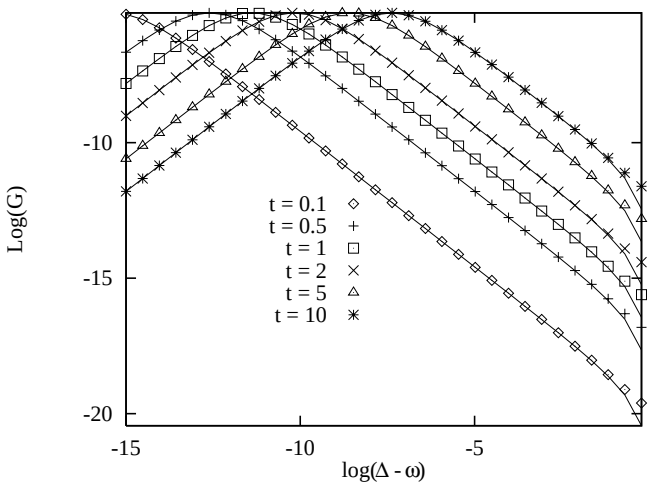

Fig. 7. The same as Figure 6 but for energies $\omega \simeq \Delta$.

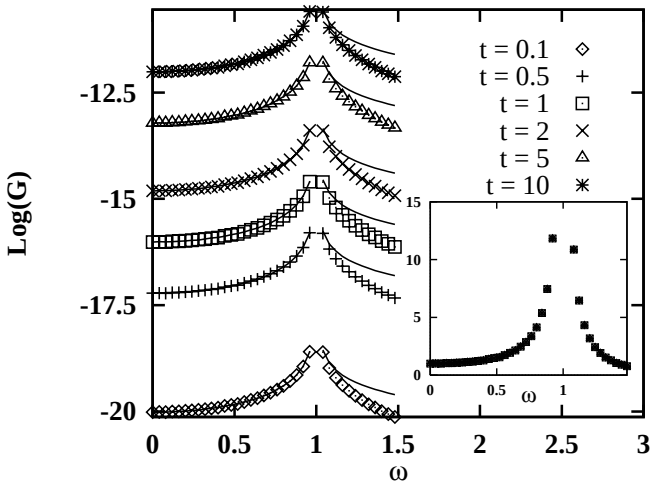

Fig. 8. Variation of the logarithm of the Andreev reflection (points) and elastic cotunneling (solid lines) conductances *versus* energy ω. We averaged the conductance over all possible phase configurations (see Eq. (56)). The insert shows the energy dependence of the rescaled conductance $\mathcal{G}(\omega)/\mathcal{G}(\omega = 0)$. The parameters are identical as in Figure 3.

The diagonal coefficient $\mathcal{G}_{a,a}$ takes the form

$$\mathcal{G}_{a,a} = -\mathcal{G}_{a,b} - \mathcal{G}_{a,c} + \frac{4\Gamma_a}{\mathcal{D}^A\mathcal{D}^R}\Big\{-\pi\rho_g\tilde{\mathcal{M}}^{a,a,A}\tilde{\mathcal{M}}^{a,a,R} \quad (52)$$

$$+\Gamma_b^2\left\{|f^{\alpha,\beta}|^2\left[|g^{\beta,\beta}|\right.\right.$$

$$\left.\left.+\Gamma_c\left(2+\Gamma_c|g^{\gamma,\gamma}|\right)\left(|g^{\beta,\beta}g^{\gamma,\gamma}| - |G^{\beta,\gamma}|^2\right)\right]\right\} \quad (53)$$

$$+\Gamma_c^2\left\{|f^{\alpha,\gamma}|^2\left[|g^{\gamma,\gamma}|\right.\right.$$

$$\left.\left.+\Gamma_b\left(2+\Gamma_b|g^{\beta,\beta}|\right)\left(|g^{\beta,\beta}g^{\gamma,\gamma}| - |g^{\beta,\gamma}|^2\right)\right]\right\} \quad (54)$$

$$+2\Gamma_b\Gamma_c|f^{\alpha,\beta}f^{\alpha,\gamma}g^{\beta,\gamma}|$$

$$\times\left[1-\Gamma_b\Gamma_c\left(|g^{\beta,\beta}g^{\gamma,\gamma}| - |g^{\beta,\gamma}|^2\right)\right]\Big\}, \quad (55)$$

and similar expressions can be obtained for $\mathcal{G}_{b,b}$ and $\mathcal{G}_{c,c}$.

6.2 Phase resolved versus average conductance

Let us now consider the special situation in which a ferromagnetic electrode with 100% spin polarization is at a distance D away from a normal metal electrode having a zero spin polarization. Namely, we assume that sites α and β coincide (see Fig. 5). This provides the simplest model containing both Andreev reflection and elastic cotunneling.

Following Section 4.4, we evaluate the phase-resolved conductance with $\varphi_{a,b} = \varphi_{a,c} = \varphi_{b,c} = \pi/2$. With this particular value of the phases, the phase-resolved conductance coincides with the effective Green's function conductance. We have shown in Figure 6 the energy dependence of the Andreev reflection and elastic tunneling conductances, evaluated with $\varphi = \pi/2$. It is visible that the Andreev reflection conductance is larger than the elastic cotunneling conductance by a factor Δ/ω. The Andreev conductance coincides with the elastic cotunneling conductance only when ω is close to Δ (see Fig. 7). This behavior can be understood from the effective Green's function conductance (Eqs. (46–48)).

To obtain the average conductance, we assume that the phase variables are independent random variables, and average the conductance over all possible values of the phases:

$$\langle\langle\mathcal{G}\rangle\rangle = \int_0^{2\pi}\frac{\mathrm{d}\varphi_{a,b}}{2\pi}\int_0^{2\pi}\frac{\mathrm{d}\varphi_{a,c}}{2\pi}\int_0^{2\pi}\frac{\mathrm{d}\varphi_{b,c}}{2\pi}\mathcal{G}(\varphi_{a,b},\varphi_{a,c},\varphi_{b,c}). \quad (56)$$

It is visible in Figure 8 that after phase averaging, the Andreev reflection conductance coincides exactly with the

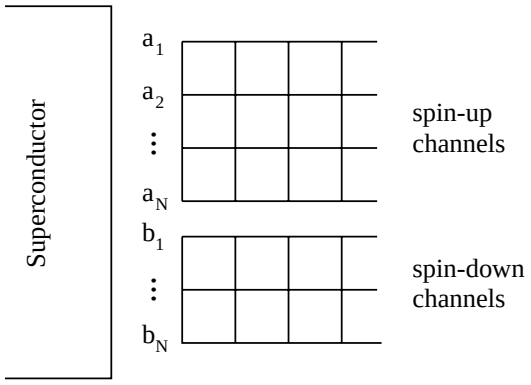

Fig. 9. Schematic representation of the tight binding model. The contacts between the spin-up ferromagnet and the superconductor are noted a_1,..., a_N. The contacts between the spin-down ferromagnet and the superconductor are noted b_1,..., b_N.

elastic cotunneling conductance below the superconducting gap. For energies close to Δ, we find again the existence of a maximum in the conductance at an energy ω^*. The predictions of perturbation theory are valid in the energy range $\omega < \omega^*$. In this energy range, all conductance spectra in Figure 8 can be deduced from each other by a simple rescaling (see the insert of Fig. 8).

7 Multichannel electrodes

7.1 Transport formula

We want to determine whether extended contacts have a physics identical to the single channel contacts considered in Sections 4, 5 and 6. We are thus lead to investigate the following situations:

(i) *The phase averaged conductance of extended contacts.* There are $N(N-1)/2$ phases $\varphi_{i,j}$ associated with a contact having N channels. The phase-averaged conductance is obtained by averaging the conductance over all possible values of these phases:

$$\langle\langle \mathcal{G} \rangle\rangle = \prod_{\langle i,j \rangle} \frac{\mathrm{d}\varphi_{i,j}}{2\pi} \mathcal{G}\left(\{\varphi_{i,j}\}\right). \tag{57}$$

(ii) *The phase-resolved conductance of extended contacts.* This is the conductance of an extended contact where the phases $\varphi_{i,j}$ are deterministic and take the particular value $\varphi_{i,j} = k_F|\mathbf{x}_i - \mathbf{x}_j|$ as given by equation (12).

Let us consider a model in which a multichannel fully polarized spin-up electrode is in contact with a superconductor. At a distance D, there is another fully polarized spin-down electrode. The tight binding model is represented in Figure 9. There is one block "a" made of N fully polarized spin-up channels and another block "b" made of M fully polarized spin-down channels. The only difference with Section 5 is the existence of a propagator g_{a_i,a_j}, g_{b_i,b_j} with $i \neq j$. The form of the Dyson matrix is still given by (B.1). Compared to (B.2), there is an additional summation in the coefficients of the Dyson matrix:

$$X^{a_i,b_j} = \sum_k g_{1,1}^{a_i,a_k} t^{a_k,\alpha_k} f^{\alpha_k,\beta_j} t^{\beta_j,b_j} \tag{58}$$

$$X^{b_i,a_j} = \sum_k g_{2,2}^{b_i,b_k} t^{b_k,\beta_k} f^{\beta_k,\alpha_j} t^{\alpha_j,a_j} \tag{59}$$

$$X^{a_i,a_j} = \sum_k g_{1,1}^{a_i,a_k} t^{a_k,\alpha_k} g^{\alpha_k,\alpha_j} t^{\alpha_j,a_j} \tag{60}$$

$$X^{b_i,b_j} = \sum_k g_{2,2}^{b_i,b_k} t^{b_k,\beta_k} g^{\beta_k,\beta_j} t^{\beta_j,b_j}. \tag{61}$$

The derivation of the transport formula is similar to Section 5. For instance, the subgap Andreev conductance is the sum of all possible Cooper pair transmissions:

$$\mathcal{G}_{a,b}^{A}(\omega) = 4\pi^2 \sum_{p\in F_a} \sum_{q\in F_b} |t^{a_p,\alpha_p}|^2 |t^{b_q,\beta_q}|^2 \rho_{1,1}^{a_p,a_p}(\omega) \rho_{2,2}^{b_q,b_q}(\omega) \times \tilde{f}^{\alpha_p,\beta_q,R}(\omega) \tilde{f}^{\beta_q,\alpha_p,A}(\omega), \tag{62}$$

where "$p \in F_a$" ("$q \in F_b$") means that the p runs over all possible channels in electrodes a and b. We used the notation

$$\tilde{f}^{\alpha_p,\beta_q} = \frac{\tilde{\mathcal{M}}^{b_q,a_p}}{t^{a_p,\alpha_p} t^{b_q,\beta_q} g_{1,1}^{a_p,a_p} \mathcal{D}} \tag{63}$$

$$\tilde{f}^{\beta_q,\alpha_p} = \frac{\tilde{\mathcal{M}}^{a_p,b_q}}{t^{a_p,\alpha_p} t^{b_q,\beta_q} g_{2,2}^{b_q,b_q} \mathcal{D}} \tag{64}$$

for the renormalized propagators. The same formalism can be used to handle more complicated situations involving an arbitrary number of electrodes having arbitrary spin polarizations.

7.2 Andreev reflection versus cotunneling

Let us consider a system in which two multichannel electrodes are in contact with a superconductor: (i) a ferromagnetic electrode; and (ii) a normal metal electrode with no spin polarization.

Following the discussion in Section 3.2, we use the ratio $l^{(\downarrow)}/l^{(\uparrow)}$ to parametrize spin polarization. There is no spin polarization if $l^{(\downarrow)}/l^{(\uparrow)} = 1$ and there is a strong spin polarization if $l^{(\downarrow)}/l^{(\uparrow)} \ll 1$. We have shown in Figure 10 the variation of the $\omega = 0$ Andreev and cotunneling phase averaged conductances as a function of spin polarization in the ferromagnetic electrode. Elastic cotunneling at $\omega = 0$ is vanishingly small if the ferromagnet is strongly polarized. The average Andreev conductance is equal to the average elastic cotunneling conductance in the absence of spin polarization (*i.e.* with $l^{(\downarrow)} = l^{(\uparrow)}$).

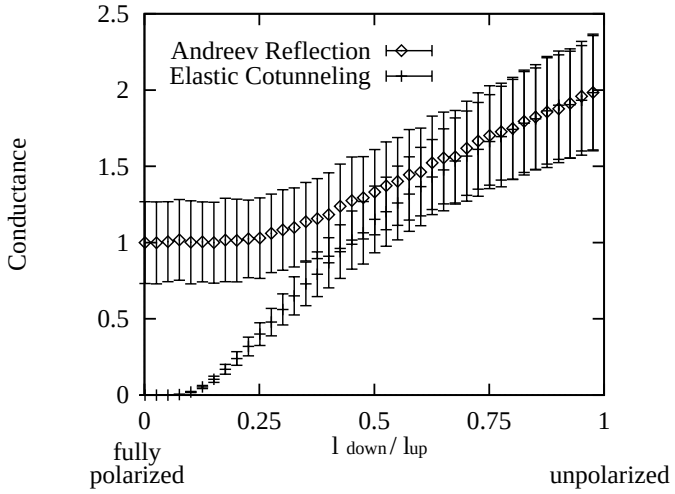

Fig. 10. Variation of the $\omega = 0$ Andreev and elastic cotunneling average conductances as a function of $l^{(\downarrow)}/l^{(\uparrow)}$. The section of the two electrodes is circular, with a radius $R = 2.1$. There are 26 channels in each electrode. The average conductances are normalized with respect to the average Andreev conductance with $\omega = 0$ and $l^{(\downarrow)} = 0$. The conductance is distributed as a function of the phases. The errorbars indicate the root mean square of the conductance distribution. The parameters are identical to Figure 3.

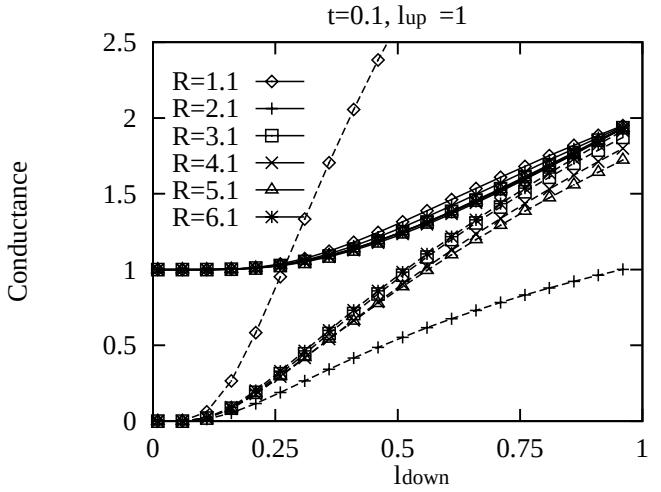

Fig. 11. Variation of the $\omega = 0$ Andreev and elastic cotunneling conductances as a function of $l^{(\downarrow)}/l^{(\uparrow)}$ for an extended contact with deterministic phases. $l^{(\downarrow)}/l^{(\uparrow)} = 1$ corresponds to a non magnetic metal. The section of the two electrodes is circular, with a radius $R = 1.1$ ($\Diamond$, 10 channels), $R = 2.1$ ($+$, 26 channels), $R = 3.1$ ($\Box$, 58 channels), $R = 4.1$ ($\times$, 98 channels), $R = 5.1$ (Δ, 178 channels), $R = 6.1$ ($*$, 242 channels). The parameters are identical to Figure 3. The normalizations are identical to Figure 10.

Therefore, the phase averaged conductance matrix of the multichannel model behaves like the phase averaged conductance matrix of the single channel model.

7.3 Extended contacts without phase averaging

Now we consider extended contacts in which the phases take deterministic values. The phases are given by equation (12): $\varphi_{i,j} = k_F|\mathbf{x}_i - \mathbf{x}_j|$. We represented in Figure 11 the dependence of the Andreev and cotunneling currents as a function of $l^{(\downarrow)}/l^{(\uparrow)}$ for $\omega = 0$. If the number of channels is sufficiently large, we see that the Andreev and elastic cotunneling conductances are almost identical for the non magnetic metal ($l^{(\downarrow)}/l^{(\uparrow)} = 1$). The behavior of extended contacts with deterministic phases (see Fig. 11) is therefore identical to the behavior of contacts with random phases (see Fig. 10). This result, already established in the perturbative regime ($\omega \ll \Delta$) is found to be valid at any frequency and barrier transparency. We have verified that this behavior is also valid in the non perturbative regime ($\omega^* < \omega < \Delta$). Notice that the same result is found if only one contact is extended, the other one having a few channels.

8 Conclusions

We have provided in this article a detailed theoretical description of ballistic transport in multiterminal hybrid structures involving a superconductor and several spin-polarized electrodes. We have performed a non perturbative calculation of the conductance matrix, using Keldysh technique, and focusing on the spin dependence, the geometry dependence and the energy behavior of the two basic processes: Crossed (intercontact) Andreev and Elastic Cotunneling. This generalizes previous perturbative calculations, valid only for low contact transparencies and at small voltages. It also generalizes non perturbative calculations made for a single contact and using effective Green's functions, which turns out to correspond to a certain choice of the phase ($\varphi = \pi/2$) in the electronic propagators.

A first issue concerns the subgap voltage dependence of the conductances, compared to the usual Andreev conductance at a single contact. A maximum is found at a crossover energy (voltage), and the conductance at this maximum is reduced compared to the ideal Andreev conductance obtained exactly at $\omega = \Delta$ in the single contact case. The higher the transparency of the barriers, the lower is this crossover energy, below which the perturbative theory is essentially valid.

The other important issue concerns the phase problem. Owing to the different forms of the normal and anomalous propagators controlling (in the superconductor) the cotunneling and Andreev processes respectively, the corresponding conductances assume different values for single-channel contacts (cotunneling takes place if they have parallel spin polarization, crossed Andreev if they have antiparallel ones). This was exemplified here in a

three-contact configuration with spin polarizations chosen such as both processes can be compared in equivalent geometries. On the other hand, averaging the Fermi phase oscillations present in the propagators make the two processes lead to equivalent conductance contributions. We have shown that a self-averaging effect occurs when at least one of the contacts has many channels. The resulting symmetry (equality of cotunneling and Andreev crossed conductances) was previously demonstrated in a perturbative regime, but it now appears as much more general. As a consequence, if at least one of the contacts is not spin-polarized, the resulting intercontact conductance is zero, by compensation of cotunneling and Andreev processes [4]. Conversely, for spin-polarized contacts this offers a way of measuring, in amplitude and direction, the polarization of one contact with respect to the other through the crossed current measurement, as proposed in reference [24]. We believe that multiterminal superconducting-ferromagnet devices have a large, yet unexplored, potential in the growing field of spintronics. Further theoretical problems concern the self-consistent calculation of the superconducting gap [10].

Appendix A: Expression of the Keldysh propagator: two-channel model

In this appendix we derive the expression of the Keldysh propagator associated to two single-channel electrodes with 100% spin polarization (see Sect. 4). We need to calculate the Keldysh component: $\hat{t}_{a,\alpha}\hat{G}^{+,-}_{\alpha,a} = \sum_{i,j}\hat{K}_{i,j}$, with $i,j \in \{a,b,\alpha,\beta\}$, and

$$\hat{K}_{\alpha,\alpha} = \hat{t}_{a,\alpha}\left[\hat{I} + \hat{G}^R_{\alpha,a}\hat{t}_{a,\alpha}\right]\hat{g}^{+,-}_{\alpha,\alpha}\hat{t}_{\alpha,a}\hat{G}^A_{a,a} \quad (A.1)$$

$$\hat{K}_{\alpha,\beta} = \hat{t}_{a,\alpha}\left[\hat{I} + \hat{G}^R_{\alpha,a}\hat{t}_{a,\alpha}\right]\hat{g}^{+,-}_{\alpha,\beta}\hat{t}_{\beta,b}\hat{G}^A_{b,a} \quad (A.2)$$

$$\hat{K}_{\beta,\alpha} = \hat{t}_{a,\alpha}\hat{G}^R_{\alpha,b}\hat{t}_{b,\beta}\hat{g}^{+,-}_{\beta,\alpha}\hat{t}_{\alpha,a}\hat{G}^A_{a,a} \quad (A.3)$$

$$\hat{K}_{\beta,\beta} = \hat{t}_{a,\alpha}\hat{G}^R_{\alpha,b}\hat{t}_{b,\beta}\hat{g}^{+,-}_{\beta,\beta}\hat{t}_{b,\beta}\hat{G}^A_{\beta,a} \quad (A.4)$$

$$\hat{K}_{a,a} = \hat{t}_{a,\alpha}\hat{G}^R_{\alpha,\alpha}\hat{t}_{\alpha,a}\hat{g}^{+,-}_{a,a}\left[\hat{I} + \hat{t}_{a,\alpha}\hat{G}^A_{\alpha,a}\right] \quad (A.5)$$

$$\hat{K}_{b,b} = \hat{t}_{a,\alpha}\hat{G}^R_{\alpha,\beta}\hat{t}_{\beta,b}\hat{g}^{+,-}_{b,b}\hat{t}_{b,\beta}\hat{G}^A_{\beta,b}. \quad (A.6)$$

We also need to calculate $\hat{t}_{\alpha,a}\hat{G}^{+,-}_{a,\alpha} = \sum_{i,j}\hat{K}'_{i,j}$, with

$$\hat{K}'_{\alpha,\alpha} = \hat{G}^R_{a,a}\hat{t}_{a,\alpha}\hat{g}^{+,-}_{\alpha,\alpha}\left[\hat{I} + \hat{t}_{\alpha,a}\hat{G}^A_{a,\alpha}\right] \quad (A.7)$$

$$\hat{K}'_{\alpha,\beta} = \hat{G}^R_{a,a}\hat{t}_{a,\alpha}\hat{g}^{+,-}_{\alpha,\beta}\hat{t}_{\beta,b}\hat{G}^A_{b,\alpha} \quad (A.8)$$

$$\hat{K}'_{\beta,\alpha} = \hat{G}^R_{a,b}\hat{t}_{b,\beta}\hat{g}^{+,-}_{\beta,\alpha}\left[\hat{I} + \hat{t}_{\alpha,a}\hat{G}^A_{a,\alpha}\right] \quad (A.9)$$

$$\hat{K}'_{\beta,\beta} = \hat{G}^R_{a,b}\hat{t}_{b,\beta}\hat{g}^{+,-}_{\beta,\beta}\hat{t}_{\beta,b}\hat{G}^A_{b,\alpha} \quad (A.10)$$

$$\hat{K}'_{a,a} = \left[\hat{I} + \hat{G}^R_{a,\alpha}\hat{t}_{\alpha,a}\right]\hat{g}^{+,-}_{a,a}\hat{t}_{a,\alpha}G^A_{\alpha,\alpha} \quad (A.11)$$

$$\hat{K}'_{b,b} = \hat{G}^R_{a,\beta}\hat{t}_{\beta,b}\hat{g}^{+,-}_{b,b}\hat{t}_{b,\beta}\hat{G}^A_{\beta,\alpha}. \quad (A.12)$$

The expression of the four terms containing $n_F(\omega-\mu_S)$ takes the form

$$\left[\hat{K}'_{\alpha,\alpha} - \hat{K}_{\alpha,\alpha}\right]_{1,1} = 4\pi^2 n_F(\omega-\mu_S)|t_{a,\alpha}|^2\rho^{a,a}_{1,1}\rho^{\alpha,\alpha}_g \times \frac{1}{\mathcal{D}^A\mathcal{D}^R}\left[1-|t_{b,\beta}|^2 g^{b,b,A}_{2,2}g^{\beta,\beta,A}\right]\times\left[1-|t_{b,\beta}|^2 g^{b,b,R}_{2,2}g^{\beta,\beta,R}\right] \quad (A.13)$$

$$\left[\hat{K}'_{\alpha,\beta} - \hat{K}_{\alpha,\beta}\right]_{1,1} = 4\pi^2 n_F(\omega-\mu_S)|t_{a,\alpha}|^2|t_{b,\beta}|^2 \times \rho^{a,a}_{1,1}\rho^{\alpha,\beta}_f g^{b,b,A}_{2,2}f^{\beta,\alpha,A} \times \frac{1}{\mathcal{D}^A\mathcal{D}^R}\left[1-|t^{b,\beta}|^2 g^{b,b,R}_{2,2}g^{\beta,\beta,R}\right] \quad (A.14)$$

$$\left[\hat{K}'_{\beta,\alpha} - \hat{K}_{\beta,\alpha}\right]_{1,1} = 4\pi^2 n_F(\omega-\mu_S)|t_{a,\alpha}|^2|t_{b,\beta}|^2 \times \rho^{a,a}_{1,1}\rho^{\beta,\alpha,A}_f g^{b,b,R}_{2,2}f^{\alpha,\beta,R} \times \frac{1}{\mathcal{D}^A\mathcal{D}^R}\left[1-|t^{b,\beta}|^2 g^{b,b,A}_{2,2}g^{\beta,\beta,A}\right] \quad (A.15)$$

$$\left[\hat{K}'_{\beta,\beta} - \hat{K}_{\beta,\beta}\right]_{1,1} = 4\pi^2 n_F(\omega-\mu_S)|t_{a,\alpha}|^2|t_{b,\beta}|^4\rho^{a,a}_{1,1}\rho^{\alpha,\beta}_g \times \frac{1}{\mathcal{D}^A\mathcal{D}^R}g^{b,b,A}_{2,2}g^{b,b,R}_{2,2}f^{\alpha,\beta,R}f^{\beta,\alpha,A}, \quad (A.16)$$

where ρ_g is one of the Nambu components of the superconductor density of states (see Eq. (6)). The terms containing μ_a and μ_b read

$$\begin{aligned}\left[\hat{K}'_{a,a} - \hat{K}_{a,a}\right]_{1,1} &= -4\pi^2 n_F(\omega-\mu_a)|t_{a,\alpha}|^2\rho^{a,a}_{1,1}\rho^{\alpha,\alpha}_g \\ &\times \frac{1}{\mathcal{D}^A\mathcal{D}^R}\left[1-|t_{b,\beta}|^2 g^{b,b,A}_{2,2}g^{\beta,\beta,A}\right]\left[1-|t_{b,\beta}|^2 g^{b,b,R}_{2,2}g^{\beta,\beta,R}\right] \\ &+ 2\mathrm{i}\pi n_F(\omega-\mu_a)|t_{a,\alpha}|^2|t_{b,\beta}|^2\rho^{a,a}_{1,1} \\ &\times \frac{1}{\mathcal{D}^A\mathcal{D}^R}g^{b,b,A}_{2,2}f^{\alpha,\beta,A}f^{\beta,\alpha,A}\left[1-|t_{b,\beta}|^2 g^{b,b,R}_{2,2}g^{\beta,\beta,R}\right] \\ &- 2\mathrm{i}\pi n_F(\omega-\mu_a)|t_{a,\alpha}|^2|t_{b,\beta}|^2\rho^{a,a}_{1,1} \\ &\times \frac{1}{\mathcal{D}^A\mathcal{D}^R}g^{b,b,R}_{2,2}f^{\alpha,\beta,R}f^{\beta,\alpha,R}\left[1-|t_{b,\beta}|^2 g^{b,b,A}_{2,2}g^{\beta,\beta,A}\right]\end{aligned} \quad (A.17)$$

$$\left[\hat{K}'_{b,b} - \hat{K}_{b,b}\right]_{1,1} = 4\pi^2 n_F(\omega-\mu_b)|t_{a,\alpha}|^2|t_{a',\alpha'}|^2 \times \rho^{a,a}_{1,1}\rho^{b,b}_{2,2}\frac{1}{\mathcal{D}^A\mathcal{D}^R}f^{\alpha,\beta,R}f^{\beta,\alpha,A}. \quad (A.18)$$

One arrives at the identity

$$\begin{aligned}&\frac{1}{n_F(\omega-\mu_S)}\left[\hat{K}'_{\alpha,\alpha} - \hat{K}_{\alpha,\alpha} + \hat{K}'_{\alpha,\beta} - \hat{K}_{\alpha,\beta} + \hat{K}'_{\beta,\alpha} - \hat{K}_{\beta,\alpha} + \hat{K}'_{\beta,\beta} - \hat{K}_{\beta,\beta}\right]_{1,1} \quad (A.19)\\ &= -\frac{1}{n_F(\omega-\mu_a)}\left[\hat{K}'_{a,a} - \hat{K}_{a,a}\right]_{1,1} - \frac{1}{n_F(\omega-\mu_b)}\left[\hat{K}'_{b,b} - \hat{K}_{b,b}\right]_{1,1}, \quad (A.20)\end{aligned}$$

which constitutes a complete derivation of the transport formula for this particular system. The expression of the Keldysh propagators given in this appendix can be used to obtain the transport formula given in Section 4.2.

Appendix B: Derivation of the transport formula with an arbitrary number of single-channel electrodes

We present in this appendix the derivation of the transport formula given by equations (38–42), associated to a situation where N ferromagnetic spin-up electrodes and M ferromagnetic spin-down electrodes are in contact with a superconductor (see Fig. 4).

B.1 Solution of the Dyson equation

The unknown Green's functions $\{G^{a_1,a_1},..., G^{a_N,a_1}, G^{b_1,a_1},..., G^{b_M,a_1}\}$ are the solution of the Dyson equation

$$\hat{\mathcal{M}} \begin{bmatrix} G^{a_1,a_1} \\ G^{a_2,a_1} \\ ... \\ G^{a_N,a_1} \\ G^{b_1,a_1} \\ ... \\ G^{b_M,a_1} \end{bmatrix} = \begin{bmatrix} g^{a_1,a_1} \\ 0 \\ ... \\ 0 \\ 0 \\ ... \\ 0 \end{bmatrix},$$

where the Dyson matrix $\hat{\mathcal{M}}$ takes the form

$$\hat{\mathcal{M}} = \hat{I} + \begin{bmatrix} -\hat{Y}^{a,a} & \hat{X}^{a,b} \\ \hat{X}^{b,a} & -\hat{Y}^{b,b} \end{bmatrix}, \tag{B.1}$$

where $\hat{Y}^{a,a}$ is a $N \times N$ block, $\hat{X}^{a,b}$ is a $N \times M$ block. The matrix elements of $\hat{X}$ and $\hat{Y}$ are

$$X^{a_i,a_j} = t^{a_i,\alpha_i} t^{a_j,\alpha_j} g^{a_i,a_j} f^{\alpha_i,\alpha_j} \tag{B.2}$$
$$Y^{a_i,a_j} = t^{a_i,\alpha_i} t^{a_j,\alpha_j} g^{a_i,a_i} g^{\alpha_i,\alpha_j}. \tag{B.3}$$

The solution of the Dyson equation takes the form

$$G^{a_i,a_j}_{1,1} = \frac{(-)^{i+j}}{\mathcal{D}} g^{a_j,a_j} \tilde{\mathcal{M}}_{a_j,a_i} \tag{B.4}$$
$$G^{b_i,b_j}_{2,2} = \frac{(-)^{i+j}}{\mathcal{D}} g^{b_j,b_j} \tilde{\mathcal{M}}_{b_j,b_i} \tag{B.5}$$
$$G^{a_i,b_j}_{1,2} = \frac{(-)^{i+j+N}}{\mathcal{D}} g^{b_j,b_j} \tilde{\mathcal{M}}_{b_j,a_i} \tag{B.6}$$
$$G^{b_i,a_j}_{2,1} = \frac{(-)^{i+j+N}}{\mathcal{D}} g^{a_j,a_j} \tilde{\mathcal{M}}_{a_j,b_i}, \tag{B.7}$$

where $\mathcal{D}$ is the determinant of the Dyson matrix and $\tilde{\mathcal{M}}_{a_i,a_j}$ are the minors of this matrix.

B.2 Solution of the Dyson-Keldysh equation

To obtain the current through the link a_1–α_1, we need to evaluate the Keldysh component

$$\hat{t}^{a_1,\alpha_1} G^{+,-}_{\alpha_1,a_1} = \hat{t}^{a_1,\alpha_1} \hat{G}^{\alpha_1,\alpha_1,R} \hat{t}^{\alpha_1,a_1} \times \hat{g}^{+,-}_{a_1,a_1} \left[\hat{I} + \hat{t}^{a_1,\alpha_1} \hat{G}^{\alpha_1,a_1,A}\right] \tag{B.8}$$
$$+ \sum_{k=2}^{N} \hat{t}^{a_1,\alpha_1} \hat{G}^{\alpha_1,\alpha_k,R} \hat{t}^{\alpha_k,a_k} \hat{g}^{+,-}_{a_k,a_k} \hat{t}^{a_k,\alpha_k} \hat{G}^{\alpha_k,a_1,A} \tag{B.9}$$
$$+ \sum_{k=1}^{N} \hat{t}^{a_1,\alpha_1} \hat{G}^{\alpha_1,\beta_k,R} \hat{t}^{\beta_k,b_k} \hat{g}^{+,-}_{b_k,b_k} \hat{t}^{b_k,\beta_k} \hat{G}^{\beta_k,a_1,A}. \tag{B.10}$$

Let us start with (B.8). The first step is to show that

$$\text{(B.8)} = 2\mathrm{i}\pi n_F(\omega - \mu_{a_1}) |t^{a_1,\alpha_1}|^2 \rho^{a_1,a_1}_{1,1} G^{\alpha_1,\alpha_1,R}_{1,1} \times \left[\hat{I} + \hat{t}^{a_1,\alpha_1} \hat{G}^{\alpha_1,\alpha_1,R}\right]_{1,1}.$$

The different terms in this equation are found to be

$$\left[\hat{I} + \hat{t}^{a_1,\alpha_1} \hat{G}^{\alpha_1,\alpha_1,R}\right]_{1,1} = \frac{\tilde{\mathcal{M}}_{a_1,a_1}}{\mathcal{D}},$$

and

$$|t^{a_1,\alpha_1}|^2 G^{\alpha_1,\alpha_1} = |t^{a_1,\alpha_1}|^2 \frac{1}{\mathcal{D}} g^{\alpha_1,\alpha_1} \tilde{\mathcal{M}}_{a_1,a_1} \tag{B.11}$$
$$+ \frac{1}{\mathcal{D}} \sum_{k \neq 1} (-)^{k+1} t^{a_1,\alpha_1} t^{a_k,\alpha_k} g^{\alpha_1,\alpha_k} \tilde{\mathcal{M}}_{a_1,a_k} \tag{B.12}$$
$$+ \frac{1}{\mathcal{D}} \sum_{k=1}^{M} (-)^{k+N} t^{a_1,\alpha_1} t^{b_k,\beta_k} f^{\alpha_1,\beta_k} \tilde{\mathcal{M}}_{a_1,b_k}. \tag{B.13}$$

To evaluate (B.9), we first show that

$$\text{(B.9)} = \sum_{k=2}^{N} 2\mathrm{i}\pi n_F(\omega - \mu_{a_k}) t^{a_1,\alpha_1} t^{a_k,\alpha_k} \rho^{a_k,a_k}_{1,1} G^{\alpha_1,\alpha_k,R}_{1,1} \times \left[\hat{t}^{a_k,\alpha_k} G^{\alpha_k,a_1}\right]^{A}_{1,1}.$$

Using the identities

$$\left[\hat{t}^{a_k,\alpha_k} G^{\alpha_k,a_1}\right]_{1,1} = (-)^{k+1} \frac{g^{a_1,a_1}}{g^{a_k,a_k}\mathcal{D}} \tilde{\mathcal{M}}_{a_1,a_k} \tag{B.14}$$
$$\left[G^{\alpha_1,\alpha_k}\right]_{1,1} = \frac{(-)^{k+1}}{t^{a_1,\alpha_1} t^{a_k,\alpha_k} g^{a_1,a_1} \mathcal{D}} \tilde{\mathcal{M}}_{a_k,a_1}, \tag{B.15}$$

we obtain

$$\text{(B.9)} = \sum_{k=2}^{N} 2\mathrm{i}\pi n_F(\omega - \mu_{a_k}) t^{a_1,\alpha_1} t^{a_k,\alpha_k} \rho^{a_k,a_k}_{1,1} g^{a_1,a_1,A} \times \tilde{g}^{R}_{\alpha_1,\alpha_k} \tilde{g}^{A}_{\alpha_k,\alpha_1},$$

where $\tilde{g}_{\alpha_1,\alpha_k}$ denotes a renormalized propagator. We use a similar calculation to evaluate (B.10) and we deduce the transport formula given by equations (38–42).

References

1. G.B. Lesovik, T. Martin, G. Blatter, Eur. Phys. J. B **24**, 287 (2001).
2. M.S. Choi, C. Bruder, D. Loss, Phys. Rev. B **62**, 13569 (2000); P. Recher, E.V. Sukhorukov, D. Loss, Phys. Rev. B **63**, 165314 (2001).
3. G. Deutscher, D. Feinberg, App. Phys. Lett. **76**, 487 (2000).
4. G. Falci, D. Feinberg, F.W.J. Hekking, Europhys. Lett. **54**, 255 (2001).
5. R. Mélin, J. Phys. Cond. Matt. **13**, 6445 (2001); R. Mélin, *Proceedings of the XXXVIth Rencontres de Moriond*, edited by T. Martin, G. Montambaux, J. Trân Thanh Vân (EDP Sciences, 2001), p. 547.
6. M.J.M. de Jong, C.W.J. Beenakker, Phys. Rev. Lett. **74**, 1657 (1995).
7. R.J. Soulen *et al.*, Science **282**, 85 (1998).
8. S.K. Upadhyay *et al.*, Phys. Rev. Lett. **81**, 3247 (1998).
9. I. Baladié, A. Buzdin, N. Ryzhanova, A. Vedyayev, Phys. Rev. B **63**, 054518 (2001); A. Buzdin, A.V. Vedyayev, N. Ryzhanova, Europhys. Lett. **48**, 686 (1999).
10. V. Apinyan, R. Mélin, Eur. Phys. J. B, to appear, `cond-mat/0107038`.
11. M. Giroud *et al.*, Phys. Rev. B **58**, R11872 (1998).
12. V.T. Petrashov, I.A. Sosnin, C. Troadec, `arXiv: cond-mat/0007278`.
13. R. Mélin, Europhys. Lett. **51**, 202 (2000).
14. J. Aumentado, V. Chandrasekhar, Phys. Rev. B **64**, 054505 (2001), `arXiv:cond-mat/0007433`.
15. W. Belzig, A. Brataas, Yu.V. Nazarov, G.E. Bauer, Phys. Rev. B **62**, 9726 (2000), `arXiv: cond-mat/0005188`.
16. J.M. Byers, M.E. Flatté, Phys. Rev. Lett. **74**, 306 (1995).
17. J.C. Cuevas, A. Martin-Rodero, A. Levy Yeyati, Phys. Rev. B **54**, 7366 (1996).
18. L.V. Keldysh, Sov. Phys. JETP **20**, 1018 (1965).
19. C. Caroli, R. Combescot, P. Nozières, D. Saint-James, J. Phys. C **4**, 916 (1971); *ibid.* **5**, 21 (1972).
20. T. Valet, A. Fert, Phys. Rev. B **48**, 7099 (1993); T. Valet, A. Fert, J. Magn. Magn. Mater. **121**, 378 (1993); A. Fert, T. Valet, J. Barnas, J. Appl. Phys. **75**, 6693 (1994); A. Fert, J.L. Duvail, T. Valet, Phys. Rev. B **52**, 6513 (1995).
21. M.A.M. Gijs, G. Bauer, Adv. Phys. **46**, 285 (1997).
22. R. Mélin, D. Denaro, Eur. Phys. J. B **18**, 149 (2000).
23. G.E. Blonder, M. Tinkham, T.M. Klapwijk, Phys. Rev. B **25**, 4515 (1982).
24. D. Feinberg, G. Deutscher, G. Falci, F. Hekking, *Proceedings of the XXXVIth Rencontres de Moriond*, edited by T. Martin, G. Montambaux, J. Trân Thanh Vân (EDP Sciences, 2001).